Editors' Suggestion | Featured in Physics

Water-Wave Vortices and Skyrmions

Daria A. Smirnova,[1,2] Franco Nori,[1,3,4] and Konstantin Y. Bliokh[1,5,6]

[1]Theoretical Quantum Physics Laboratory, Cluster for Pioneering Research, RIKEN, Wako-shi, Saitama 351-0198, Japan
[2]Research School of Physics, Australian National University, Canberra, Australian Capital Territory 2601, Australia
[3]Center for Quantum Computing (RQC), RIKEN, Wako-shi, Saitama 351-0198, Japan
[4]Physics Department, University of Michigan, Ann Arbor, Michigan 48109-1040, USA
[5]Centre of Excellence ENSEMBLE3 Sp. z o.o., 01-919 Warsaw, Poland
[6]Donostia International Physics Center (DIPC), Donostia-San Sebastián 20018, Spain

(Received 10 August 2023; accepted 14 November 2023; published 31 January 2024)

Topological wave structures—phase vortices, skyrmions, merons, etc.—are attracting enormous attention in a variety of quantum and classical wave fields. Surprisingly, these structures have never been properly explored in the most obvious example of classical waves: water-surface (gravity-capillary) waves. Here, we fill this gap and describe (i) water-wave vortices of different orders carrying quantized angular momentum with orbital and spin contributions, (ii) skyrmion lattices formed by the instantaneous displacements of the water-surface particles in wave interference, and (iii) meron (half-skyrmion) lattices formed by the spin-density vectors, as well as (iv) spatiotemporal water-wave vortices and skyrmions. We show that all these topological entities can be readily generated in linear water-wave interference experiments. Our findings can find applications in microfluidics and show that water waves can be employed as an attainable playground for emulating universal topological wave phenomena.

DOI: 10.1103/PhysRevLett.132.054003

Introduction.—Wave vortices are universal physical entities with nontrivial topological and dynamical properties: quantized phase increments around point phase singularities and quantumlike angular momentum (AM). Examples of wave vortices have been known since the 19th century; these have been observed and explored in tidal [1], quantum-fluid [2,3], optical [4–6], sound [7–9], elastic [10], surface-plasmon [11,12], exciton-polariton [13], quantum-electron [14], neutron [15], and atom [16] waves.

Strikingly, wave vortices have not been properly studied in the most obvious example of classical waves: water-surface (gravity-capillary) waves. Only a recent series of experiments [17–20] described the generation of a square lattice of alternating vortices in the interference of orthogonal standing water waves.

However, the theoretical description of these experiments lacks the identification with *wave vortices*, very different from the usual hydrodynamical vortices. It was indicated that the hydrodynamical vorticity appears due to nonlinearity [17,18] and that these vortices are closely related to the Stokes drift and AM [19,20], but no quantized topological and dynamical properties have been indicated. Furthermore, only the simplest first-order vortices were produced (cf., e.g., quantum-electron vortices of higher orders $\sim 10^2$–10^3 [21,22]).

In this Letter, we describe water-wave vortices (WWVs) in gravity-capillary waves. We reveal their topological properties and show that circularly symmetric vortices are eigenmodes of the *total AM* operator, including the spin and orbital parts. In the linear approximation, WWVs have *zero vorticity*. Nonetheless, the quadratic *Stokes drift* produces slow orbital motion of water particles and nonzero nonlinear vorticity. Importantly, water particles experience two kinds of circular motions with different spatial and temporal scales: (i) local linear-amplitude-scale circular motion with the wave frequency in the linear regime and (ii) slow wavelength-scale circular motion due to the nonlinear Stokes drift. These two motions are responsible for the spin and orbital contributions to the quantized total AM.

Moreover, water waves have inherent *vector* properties: The local Eulerian displacement of water-surface particles is a counterpart of the 3D polarization in optical or acoustic wave fields [23,24]. Therefore, following great recent progress in the generation of topological vector entities—*skyrmions* [25]—in classical electromagnetic [26–32], sound [33,34], and elastic [35] waves, here we describe *water-wave skyrmions*. We show that the interference of three plane water waves can generate a hexagonal lattice of (i) WWVs, (ii) skyrmions of the instantaneous water-particle displacements, and (iii) *merons* (half-skyrmions) of the local spin density. This field configuration is just one step from the recent experiments [17–20] and is quite feasible for the experimental implementation.

Finally, following enormous current interest in *spacetime* structured waves [36,37], in particular, *spatiotemporal vortices* [38–42], we show that, by detuning the frequency of one of the interfering waves, one can readily produce

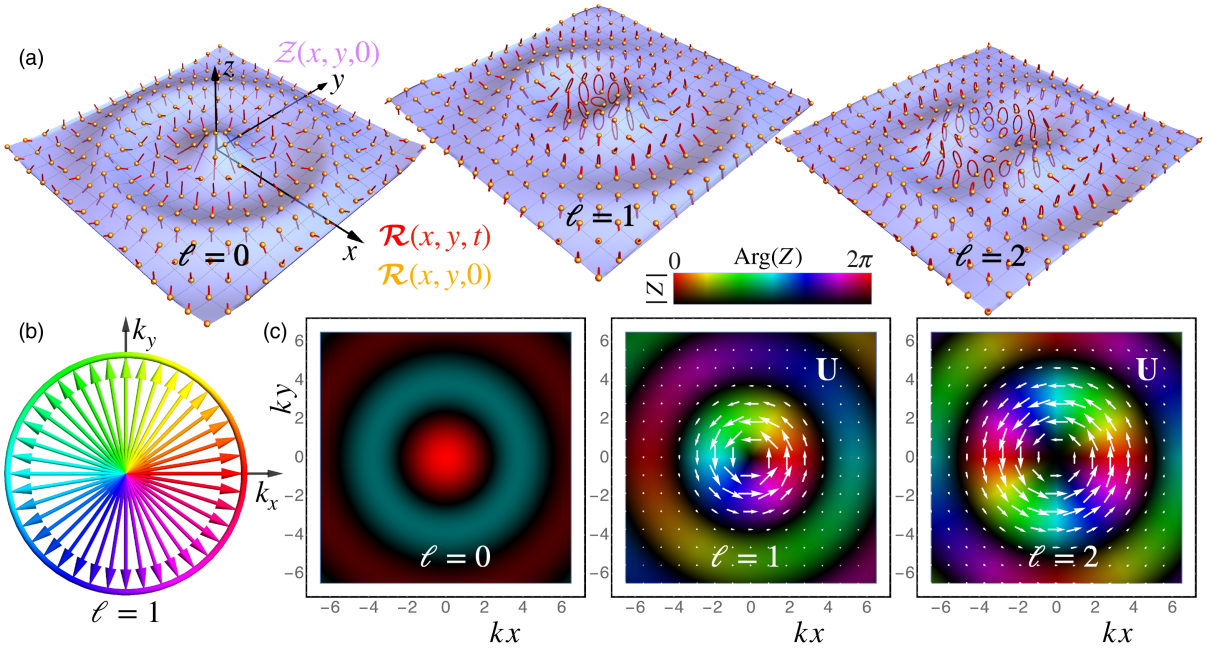

FIG. 1. (a) Instantaneous water surfaces $\mathcal{Z}(x,y,0)$ and Eulerian water-surface particle trajectories $\boldsymbol{\mathcal{R}}(x,y,t)$ for circular WWVs with different topological charges ℓ [Eqs. (2) and (3)]. The spin density $\mathbf{S}$ is directed normally to the elliptical particle trajectories and quantifies the AM of this elliptical motion. (b) The plane-wave spectrum of a circular WWV with color-coded phases for $\ell=1$. (c) The complex vertical-displacement field $Z(x,y)$ for WWVs from panel (a), with the phases and amplitudes coded by the colors and brightness, respectively. The white arrows indicate the second-order Stokes drift $\mathbf{U}$ [Eq. (6)], characterizing the wave momentum density.

moving lattices of spatiotemporal WWVs and *spatiotemporal skyrmions*.

Thus, we reveal new structures with remarkable topological and dynamical properties in linear water waves. We argue that water waves offer a perfect classical platform for emulating universal quantum and topological wave phenomena, which can also find useful applications in microfluidics [43,44].

Water-wave vortices.—We first consider monochromatic gravity-capillary waves on a deep-water surface. The 3D Eulerian displacement of the water particles from the $z=0$ surface is $\boldsymbol{\mathcal{R}}(\mathbf{r}_2,t)=\mathrm{Re}[\mathbf{R}(\mathbf{r}_2)e^{-i\omega t}]=(\mathcal{X},\mathcal{Y},\mathcal{Z})$, where $\mathbf{R}=(X,Y,Z)$ is the complex displacement wave field, $\mathbf{r}_2=(x,y)$, and ω is the frequency. Separating the vertical and in-plane components of 3-vectors as $\mathbf{a}\equiv(a_x,a_y,a_z)=(\mathbf{a}_2,a_z)$, the wave equations of motion can be written as [20,45]

$$\omega^2\mathbf{R}_2=\left(g-\frac{\alpha}{\rho}\Delta_2\right)\boldsymbol{\nabla}_2 Z,$$
$$\omega^2 Z=-\left(g-\frac{\alpha}{\rho}\Delta_2\right)\boldsymbol{\nabla}_2\cdot\mathbf{R}_2. \tag{1}$$

Here, g is the gravitational acceleration, α is the surface-tension coefficient, ρ is the water density, $\Delta_2=\boldsymbol{\nabla}_2\cdot\boldsymbol{\nabla}_2$, and Eqs. (1) with the plane-wave ansatz $\boldsymbol{\nabla}_2\to i\mathbf{k}$ ($\mathbf{k}$ is the wave vector) yield the dispersion relation $\omega^2=gk+(\alpha/\rho)k^3$.

The vortex solutions of Eqs. (1) are obtained as a superposition of plane waves with wave vectors uniformly distributed along the $k_x^2+k_y^2=k^2$ circle with the azimuthal phase increment $2\pi\ell$, $\ell\in\mathbb{Z}$ [Fig. 1(b)]. Constructing the complex vertical displacement in this way, we obtain

$$Z=\frac{A}{2\pi}\int_0^{2\pi}e^{i\mathbf{k}\cdot\mathbf{r}_2+i\ell\phi}d\phi=AJ_\ell(kr)e^{i\ell\varphi}. \tag{2}$$

Here, A is a constant wave amplitude, J_ℓ is the Bessel function of the first kind, and ϕ is the azimuthal angle in the (k_x,k_y) plane, whereas (r,φ) are the polar coordinates in the (x,y) plane.

Equation (2) describes 2D scalar cylindrical Bessel waves [Fig. 1(c)]. However, water waves have a vectorial nature, and the other two components of the wave field can be found from the first Eq. (1). It is convenient to write these in the basis of "circular polarizations" [46,47]:

$$R^\pm\equiv\frac{X\mp iY}{\sqrt{2}}=\pm\frac{A}{\sqrt{2}}J_{\ell\mp1}(kr)e^{i(\ell\mp1)\varphi}. \tag{3}$$

In this basis, the z component of the spin-1 operator, universal for classical vector waves, reads $\hat{S}_z=\mathrm{diag}(1,-1,0)$, while the z component of the orbital AM (OAM)

operator is $\hat{L}_z = -i\partial_\varphi$ [5]. Introducing the "wave function" $|\psi\rangle = (R^+, R^-, Z)$, one can see that the WWVs (2) and (3) are *not* the OAM eigenmodes, but these are eigenmodes of the z component of the *total* AM with the quantized eigenvalue ℓ:

$$\hat{J}_z|\psi\rangle = (\hat{L}_z + \hat{S}_z)|\psi\rangle = \ell|\psi\rangle. \tag{4}$$

Such behavior (which can be interpreted as the inherent spin-orbit coupling) is a common feature of all cylindrical vector waves: optical [46,48,49], quantum [50], acoustic [51], and elastic [47].

Figure 1(a) shows instantaneous water surfaces $\mathcal{Z}(\mathbf{r}_2, 0)$ and water-particle trajectories $\boldsymbol{\mathcal{R}}(\mathbf{r}_2, t)$ for WWVs with different ℓ. The water-particle trajectories are 3D ellipses, entirely similar to the electric-field polarization in optical fields [24]. The normal to the ellipse and its ellipticity determine the cycle-averaged AM of the particle, i.e., *spin density* in water waves [20,52]: $\mathbf{S} = (\rho\omega/2)\mathrm{Im}(\mathbf{R}^* \times \mathbf{R})$. One can see that WWVs are characterized by inhomogeneous polarization textures. In the vortex center $r = 0$, the polarization is purely vertical, $|\psi\rangle \propto (0,0,1)$, for $\ell = 0$; it is purely circular, $|\psi\rangle \propto (1,0,0)$ and $|\psi\rangle \propto (0,1,0)$, for $\ell = \pm 1$; and the vector wave field vanishes, $|\psi\rangle \propto (0,0,0)$, for $|\ell| > 1$ (the vanishing of all vector wave field components requires a higher-order degeneracy [46,47,49–51,53]).

Importantly, WWVs are *not* the usual hydrodynamical vortices, which are formed by steady water motion with a nonzero circulation of the velocity $\boldsymbol{\mathcal{V}} = \partial_t \boldsymbol{\mathcal{R}}$ and vorticity $\boldsymbol{\nabla} \times \boldsymbol{\mathcal{V}} \neq \mathbf{0}$ [54]. In contrast, linear monochromatic gravity-capillary waves have zero vorticity: $\boldsymbol{\nabla} \times \mathbf{V} = \mathbf{0}$, where $\mathbf{V} = -i\omega\mathbf{R}$ is the complex velocity field. This follows from Eqs. (1) and the incompressibility equation $\boldsymbol{\nabla} \cdot \mathbf{V} = 0$. Wave vortices are *topological* entities with *quantized phase singularities* in the center. The "topological charge" can be defined in two equivalent ways [55,56]:

$$\frac{1}{2\pi}\oint \boldsymbol{\nabla}_2 \mathrm{Arg}(Z) \cdot d\mathbf{r}_2 = \frac{1}{4\pi}\oint \boldsymbol{\nabla}_2 \mathrm{Arg}(\mathbf{R}\cdot\mathbf{R}) \cdot d\mathbf{r}_2 = \ell, \tag{5}$$

where the contour integral is taken along a circuit enclosing the vortex center. These relations show that the center of the first-order $|\ell| = 1$ WWV can be considered as the first-order phase singularity in the scalar field $Z(x,y)$ or the second-order polarization singularity (C point of circular polarization) in the vector field $\mathbf{R}(x,y)$ [24,55–57]. Any perturbation breaking the cylindrical symmetry splits the second-order C point into a pair of the first-order C points, with topologically robust Möbius-strip orientations of the polarization ellipses around these points [24,34,56,58,59].

Nonzero vorticity and circulation do appear in WWVs but in the *quadratic* corrections to linear wave solutions. Namely, water particles experience a slow *Stokes drift*, i.e., the difference between the Lagrangian and Euler velocities [20,60,61]:

$$\mathbf{U} = \frac{\omega}{2}\mathrm{Im}[\mathbf{R}^* \cdot (\boldsymbol{\nabla}_2)\mathbf{R}]. \tag{6}$$

Multiplied by the mass density, it yields the canonical *wave momentum* ("pseudomomentum") density [20,62–65]: $\mathbf{P} = \rho\mathbf{U}$.

Figure 1(c) shows the azimuthal Stokes-drift flow in WWVs. It is mostly localized near the first radial maximum of the Bessel function $J_\ell(kr)$ and determines the z-directed OAM density: $\mathbf{L} = \mathbf{r}_2 \times \mathbf{P}$, $L_z = (\rho\omega/2)\mathrm{Im}(\mathbf{R}^* \cdot \partial_\varphi \mathbf{R})$. Notably, the local circular motion of water particles (spin) and the global Stokes-drift circulation (OAM) have very different space and timescales: the linear-wave amplitude A and angular frequency ω vs the wavelength $k^{-1} \gg A$ and angular velocity $U/r \sim \omega k^2 A^2 \ll \omega$. The spin and OAM densities in the WWVs (2) and (3) satisfy the relation following from Eq. (4) [47,51]:

$$J_z = L_z + S_z = \frac{\rho\omega}{2}\ell|\mathbf{R}|^2 = 2\frac{\ell}{\omega}T, \tag{7}$$

where $T = \rho|\mathbf{V}|^2/4$ is the cycle-averaged kinetic energy density.

Thus, WWVs are naturally described by a quantum-like formalism and possess nontrivial topological properties. Recent experiments [17–20] generated square lattices of alternating first-order vortices with $\ell = \pm 1$ by interfering orthogonal standing waves with the $\pi/2$ phase difference. The orbital Stokes drift and circular polarization (spin) in the vortex centers were clearly observed in Refs. [19,20], but quantized topological properties of these vortices have not been described. Higher-order WWVs with $|\ell| > 1$, which have never been observed, could provide areas of unperturbed water surface surrounded by intense circular waves and orbital Stokes flows.

Water-wave skyrmions and merons.—The 3D vector nature of water waves allows the generation of topological vector textures, such as skyrmions or merons [25–28,30–35]. Such textures can be produced by interfering several plane waves with the same frequency and wave vectors $\mathbf{k}_j = k(\cos\phi_j, \sin\phi_j, 0)$, $j = 1, \ldots, N$:

$$\mathbf{R} = \sum_{j=1}^{N} \mathbf{R}_{0j} e^{i\mathbf{k}_j\cdot\mathbf{r} + i\Phi_j}, \quad \mathbf{R}_{0j} = A_j(i\cos\phi_j, i\sin\phi_j, 1), \tag{8}$$

where A_j and Φ_j are the real-valued amplitudes and phases of the interfering waves, respectively.

Consider, for example, $N = 3$ waves, uniformly distributed with $\phi_j = 2\pi(j-1)/N$, $A_j = A$, and vortex phases

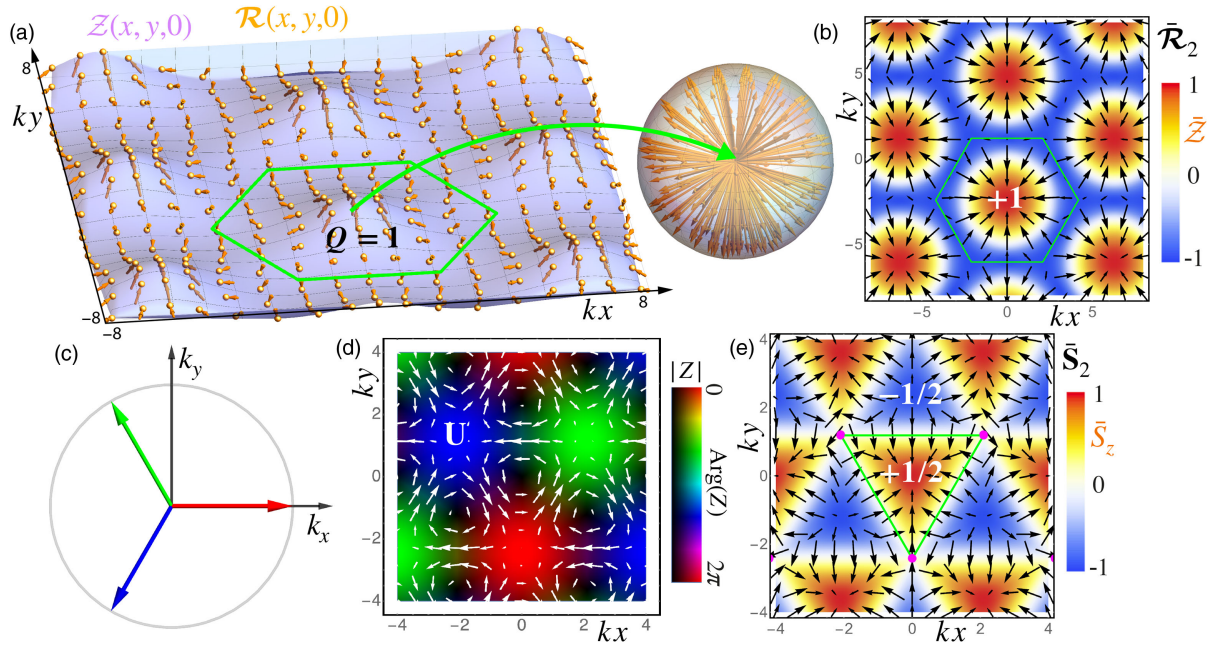

FIG. 2. Hexagonal lattice produced by the interference of three waves with equal frequencies, amplitudes, and color-coded phases shown in (c). (a) Instantaneous water surface $\mathcal{Z}(x,y,0)$ and water-surface particle displacements $\boldsymbol{\mathcal{R}}(x,y,0)$ for the field (9). The displacement directions in the unit hexagonal cell is mapped onto the unit sphere, providing a skyrmion with the topological charge $Q=1$ [Eq. (10)]. (b) The unit displacement-direction field $\bar{\boldsymbol{\mathcal{R}}}(x,y,0)$ represented by colors (vertical component $\bar{\mathcal{Z}}$) and black arrows (in-plane components $\bar{\boldsymbol{\mathcal{R}}}_2$). (d) The complex vertical-displacement field $Z(x,y)$ and the Stokes drift $\mathbf{U}$ indicating the lattice of alternating WWVs with $\ell=\pm1$. (e) The unit spin-density field $\bar{\mathbf{S}}(x,y)$ represented similar to (b). The hexagonal unit cell is split into triangular zones of spin merons (half-skyrmions) with topological charges $Q_S=\pm1/2$ and centers with $\bar{S}_z=\pm1$ corresponding to the $\ell=\pm1$ vortices in (d).

$\Phi_j=\phi_j$ [Fig. 2(c)]. These waves form a hexagonal periodic lattice with the displacement field

$$\begin{pmatrix} X \\ Y \\ Z \end{pmatrix} \propto A \begin{pmatrix} ie^{ikx}+ie^{-i(kx/2)}\sin\left(\frac{\sqrt{3}ky}{2}+\frac{\pi}{6}\right) \\ -\sqrt{3}e^{-i(kx/2)}\cos\left(\frac{\sqrt{3}ky}{2}+\frac{\pi}{6}\right) \\ e^{ikx}-2e^{-i(kx/2)}\sin\left(\frac{\sqrt{3}ky}{2}+\frac{\pi}{6}\right) \end{pmatrix}. \quad (9)$$

This field exhibits a number of topological features. First, it contains a lattice of WWVs with alternating topological charges $\ell=\pm1$ [Fig. 2(d)]. Such vortex lattices are well known in optics [66].

Second, Fig. 2(a) shows the instantaneous water surface $\mathcal{Z}(\mathbf{r}_2,0)$ and the surface-particle displacements $\boldsymbol{\mathcal{R}}(\mathbf{r}_2,0)$ for the field (9). The displacements in a hexagonal unit cell of the lattice contain all possible directions and can be mapped onto a unit sphere. This is a signature of a skyrmion, which can be characterized by the topological number

$$Q=\frac{1}{4\pi}\int\!\!\int_{\text{u.c.}}\bar{\boldsymbol{\mathcal{R}}}\cdot[\partial_x\bar{\boldsymbol{\mathcal{R}}}\times\partial_y\bar{\boldsymbol{\mathcal{R}}}]dxdy, \quad (10)$$

where $\bar{\boldsymbol{\mathcal{R}}}=\boldsymbol{\mathcal{R}}/|\boldsymbol{\mathcal{R}}|$. In the case under consideration, $Q=1$ at $t=0$, but it can change its sign over time, because the displacement evolves and becomes opposite after half a period, $t=\pi/\omega$ [34]. Figure 2(b) displays another representation of the skyrmion lattice, where colors and black vectors indicate the z and (x,y) components, respectively, of the displacement-direction field $\bar{\boldsymbol{\mathcal{R}}}$. Moving from the center of the cell toward its boundary, the vector $\bar{\boldsymbol{\mathcal{R}}}$ undergoes a rotation, where its z component changes sign, resulting in a nontrivial winding captured by the nonzero skyrmion charge Q. Similar skyrmion lattices have been observed in electromagnetic [26], sound [33,34], and elastic [35] vector wave fields.

Third, instead of the instantaneous vector field $\boldsymbol{\mathcal{R}}$, one can trace the spin-density vector $\mathbf{S}$ (normal to the local polarization ellipse). Figure 2(e) displays the distribution of the unit spin vector $\bar{\mathbf{S}}=\mathbf{S}/|\mathbf{S}|$ in the field (9). The unit hexagonal cell is split into triangular zones with $\bar{S}_z>0$ and $\bar{S}_z<0$ separated by $\bar{S}_z=0$ lines and singular $\mathbf{S}=\mathbf{0}$ vertices. The centers of these triangles with $\bar{S}_z=\pm1$ (i.e., circular in-plane polarizations) correspond to the centers of WWVs with $\ell=\pm1$ [Fig. 2(d)] [20]. Calculating the topological charges (10) for the spin field $\bar{\mathbf{S}}$, we obtain $Q_S=\mp1/2$ for the triangular zones with $\bar{S}_z\lessgtr0$. Such topological textures are called merons or half-skyrmions, because the spin directions in each zone covers the upper or lower semisphere. Similar spin merons have been observed in electromagnetic waves [28,31,67,68].

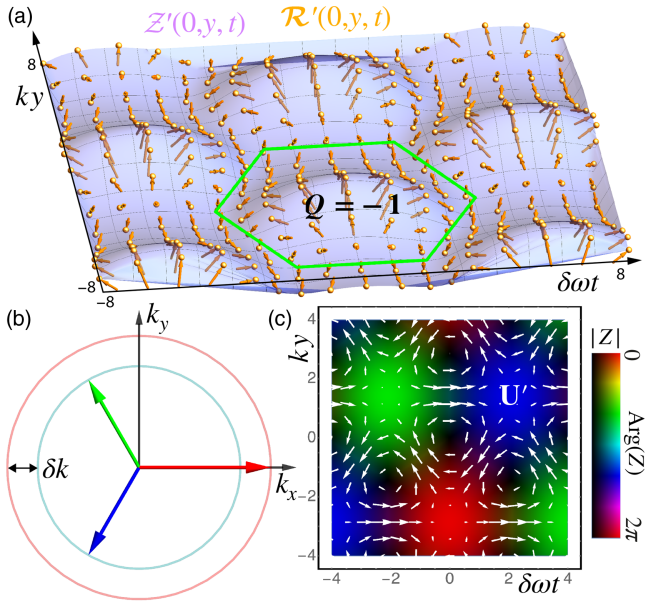

FIG. 3. The same as in Figs. 2(a), 2(c), and 2(d) but for the lattice of spatiotemporal WWVs and skyrmions. The frequency of one of the interfering waves is detuned by $\delta\omega$ and the corresponding δk. The complex vertical-displacement field Z and the real field envelope $\mathcal{R}' = \mathrm{Re}[\mathbf{R}]$ (without fast oscillations $e^{-i\omega t}$) are plotted over the spacetime domain (t, y) at the fixed coordinate $x = 0$. The temporal component of the spatiotemporal Stokes drift $\mathbf{U}' = (U_t, U_y)$ is defined as $U_t = (k\omega/2\delta\omega)\mathrm{Im}[\mathbf{R}^* \cdot (\partial_t)\mathbf{R}]$.

Here, we showed only one simple example of the water-wave interference field. WWVs, field skyrmions, and spin merons are rather universal topological entities and appear in many other fields. A square lattice formed by two standing waves [17–20] contains vortices and spin merons (cf. [31,67]), a hexagonal lattice formed by three standing waves produces field skyrmions [45], and the zero-order $\ell = 0$ Bessel mode [Eqs. (2) and (3) and Fig. 1] contains a field skyrmion (cf. [26,32]).

Spatiotemporal vortices and skyrmions.—Finally, we demonstrate another class of topological entities which can be readily generated in water waves: spatiotemporal vortices [38–42] and skyrmions. It is sufficient to slightly detune the frequency of one of the three interfering plane waves in Fig. 2: $\omega_1 \to \omega + \delta\omega$, $k_1 \to k + \delta k = (\omega + \delta\omega)^2/g$ (for simplicity, here we neglect capillarity, $\alpha \to 0$) [Fig. 3(b)]. This transforms the wave field (8) as $\Phi_1 \to \Phi_1 - i\delta\omega t$, so that the spatial lattice in Fig. 2 becomes *moving* along the x axis, and the field becomes a function of space and *time*: $\mathbf{R}(\mathbf{r}_2, t)$.

The real displacement field is $\mathcal{R}(\mathbf{r}_2, t) = \mathrm{Re}[\mathbf{R}(\mathbf{r}_2, t)e^{-i\omega t}]$, but we will analyze the field $\mathcal{R}'(\mathbf{r}_2, t) = \mathrm{Re}[\mathbf{R}(\mathbf{r}_2, t)]$ subtracting the common fast oscillations $e^{-i\omega t}$. Plotting the complex field Z and real field $\mathcal{R}'$ in the spacetime domain (t, y) at fixed $x = 0$, we find that they exhibit a scaled hexagonal lattice of vortices and skyrmions (Fig. 3). These spatiotemporal WWVs and skyrmions have opposite topological charges ℓ and Q compared to their spatial counterparts in Fig. 2.

Conclusions.—We have analyzed the fundamental topologically nontrivial objects in linear water-surface (gravity-capillary) waves, namely, WWVs, surface-particle displacement skyrmions, and spin-density merons, as well as spatiotemporal WWVs and skyrmions. All these objects are universal across different types of waves and require only standard wave-interference ingredients: relative phases and amplitudes, polarizations, and spectral detuning, to control the geometry and topology of the field. For simplicity, we considered the deep-water approximation; the finite-depth effects in monochromatic water waves produce global scaling of the vertical component on the surface: $Z \to \tanh(kH)Z$, where H is the water depth [45].

Notably, the vector features of water waves (displacement fields) are directly observable, while in other fields these are usually measured via various indirect methods. Therefore, water waves offer an attractive platform for emulating topologically nontrivial field structures and wave phenomena in a unified fashion. Furthermore, nontrivial dynamical properties of topological water-wave objects—circulating Stokes-drift currents, fast circular motions (spin) in the centers of the first-order WWVs, vanishing fields in the centers of higher-order WWVs, etc.—can be attractive for fluid-mechanical applications, such as manipulations of particles [43,44]. Finally, we note that, while most of the attention in water-wave physics has focused on nonlinear and high-amplitude effects [69–71], our study shows that wave structures around field zeros and linear-wave interference exhibit a rich variety of largely unexplored phenomena.

Note added.—After the submission of this work, more publications on WWV lattices, related to Refs. [17–20], came to our attention [72–74].

This work is supported in part by the Japan Society for the Promotion of Science (JSPS); Japan Science and Technology (JST); Nippon Telegraph and Telephone Corporation (NTT) Research; the Office of Naval Research (ONR); the Asian Office of Aerospace Research and Development (AOARD) [Grant No. FA2386-20-1-4069]; the International Research Agendas Programme (IRAP) of the Foundation for Polish Science cofinanced by the European Union under the European Regional Development Fund and Teaming Horizon 2020 program of the European Commission [ENSEMBLE3 Project No. MAB/2020/14]; the TEAM program of the Foundation for Polish Science cofinanced by the European Union under the European Regional Development Fund [Grant No. TEAM/2016-3/29]; and the Australian Research Council [FT230100058].

[1] J. F. Nye, J. V. Hajnal, and J. H. Hannay, Phase saddles and dislocations in two-dimensional waves such as the tides, Proc. R. Soc. A **417**, 7 (1988).

[2] E. J. Yarmchuk, M. J. V. Gordon, and R. E. Packard, Observation of stationary vortex arrays in rotating superfluid helium, Phys. Rev. Lett. **43**, 214 (1979).

[3] A. L. Fetter, Rotating trapped Bose-Einstein condensates, Rev. Mod. Phys. **81**, 647 (2009).

[4] M. V. Berry, *Les Houches Lecture Series Session XXXV* (North-Holland, Amsterdam, 1981), Chap. Singularities in Waves and Rays, p. 453.

[5] *Optical Angular Momentum*, edited by L. Allen, S. M. Barnett, and M. J. Padgett (IOP Publishing, Bristol, 2003).

[6] M. S. Soskin and M. V. Vasnetsov, Singular optics, Prog. Opt. **42**, 219 (2001).

[7] B. T. Hefner and P. L. Marston, An acoustical helicoidal wave transducer with applications for the alignment of ultrasonic and underwater systems, J. Acoust. Soc. Am. **106**, 3313 (1999).

[8] K. Volke-Sepulveda, A. O. Santillan, and R. R. Boullosa, Transfer of angular momentum to matter from acoustical vortices in free space, Phys. Rev. Lett. **100**, 024302 (2008).

[9] S. Guo, Z. Ya, P. Wu, and M. Wan, A review on acoustic vortices: Generation, characterization, applications and perspectives, J. Appl. Phys. **132**, 210701 (2022).

[10] G. J. Chaplain, J. M. De Ponti, and T. A. Starkey, Elastic orbital angular momentum transfer from an elastic pipe to a fluid, Commun. Phys. **5**, 279 (2022).

[11] Y. Gorodetski, A. Niv, V. Kleiner, and E. Hasman, Observation of the spin-based plasmonic effect in nanoscale structures, Phys. Rev. Lett. **101**, 043903 (2008).

[12] E. Prinz, M. Hartelt, G. Spektor, M. Orenstein, and M. Aeschlimann, Orbital angular momentum in nanoplasmonic vortices, ACS Photonics **10**, 340 (2023).

[13] R. Dall, M. D. Fraser, A. S. Desyatnikov, G. Li, S. Brodbeck, M. Kamp, C. Schneider, S. Höfling, and E. A. Ostrovskaya, Creation of orbital angular momentum states with chiral polaritonic lenses, Phys. Rev. Lett. **113**, 200404 (2014).

[14] K. Y. Bliokh, I. P. Ivanov, G. Guzzinati, L. Clark, R. Van Boxem, A. Beche, R. Juchtmans, M. A. Alonso, P. Schattschneider, F. Nori, and J. Verbeeck, Theory and applications of free-electron vortex states, Phys. Rep. **690**, 1 (2017).

[15] C. W. Clark, R. Barankov, M. G. Huber, M. Arif, D. G. Cory, and D. A. Pushin, Controlling neutron orbital angular momentum, Nature (London) **525**, 504 (2015).

[16] A. Luski, Y. Segev, R. David, O. Bitton, H. Nadler, A. R. Barnea, A. Gorlach, O. Cheshnovsky, I. Kaminer, and E. Narevicius, Vortex beams of atoms and molecules, Science **373**, 1105 (2021).

[17] S. V. Filatov, S. A. Aliev, A. A. Levchenko, and D. A. Khramov, Generation of vortices by gravity waves on a water surface, JETP Lett. **104**, 702 (2016).

[18] S. V. Filatov, V. M. Parfenyev, S. S. Vergeles, M. Yu. Brazhnikov, A. A. Levchenko, and V. V. Lebedev, Nonlinear generation of vorticity by surface waves, Phys. Rev. Lett. **116**, 054501 (2016).

[19] N. Francois, H. Xia, H. Punzmann, P. W. Fontana, and M. Shats, Wave-based liquid-interface metamaterials, Nat. Commun. **8**, 14325 (2017).

[20] K. Y. Bliokh, H. Punzmann, H. Xia, F. Nori, and M. Shats, Field theory spin and momentum in water waves, Sci. Adv. **8**, eabm1295 (2022).

[21] B. J. McMorran, A. Agrawal, I. M. Anderson, A. A. Herzing, H. J. Lezec, J. J. McClelland, and J. Unguris, Electron vortex beams with high quanta of orbital angular momentum, Science **331**, 192 (2011).

[22] A. H. Tavabi, P. Rosi, A. Roncaglia, E. Rotunno, M. Beleggia, P.-H. Lu, L. Belsito, G. Pozzi, S. Frabboni, P. Tiemeijer, R. E. Dunin-Borkowski, and V. Grillo, Generation of electron vortex beams with over 1000 orbital angular momentum quanta using a tunable electrostatic spiral phase plate, Appl. Phys. Lett. **121**, 073506 (2022).

[23] D. Sugic, M. R. Dennis, F. Nori, and K. Y. Bliokh, Knotted polarizations and spin in 3D polychromatic waves, Phys. Rev. Res. **2**, 042045(R) (2020).

[24] K. Y. Bliokh, M. A. Alonso, D. Sugic, M. Perrin, F. Nori, and E. Brasselet, Polarization singularities and Möbius strips in sound and water-surface waves, Phys. Fluids **33**, 077122 (2021).

[25] N. Nagaosa and Y. Tokura, Topological properties and dynamics of magnetic skyrmions, Nat. Nanotechnol. **8**, 899 (2013).

[26] S. Tsesses, E. Ostrovsky, K. Cohen, B. Gjonaj, N. H. Lindner, and G. Bartal, Optical skyrmion lattice in evanescent electromagnetic fields, Science **361**, 993 (2018).

[27] L. Du, A. Yang, A. V. Zayats, and X. Yuan, Deep-subwavelength features of photonic skyrmions in a confined electromagnetic field with orbital angular momentum, Nat. Phys. **15**, 650 (2019).

[28] Y. Dai, Z. Zhou, A. Ghosh, R. S. K. Mong, A. Kubo, C.-B. Huang, and H. Petek, Plasmonic topological quasiparticle on the nanometre and femtosecond scales, Nature (London) **588**, 616 (2020).

[29] S. Gao, F. C. Speirits, F. Castellucci, S. Franke-Arnold, S. M. Barnett, and J. B. Götte, Paraxial skyrmionic beams, Phys. Rev. A **102**, 053513 (2020).

[30] Y. Shen, Y. Hou, N. Papasimakis, and N. I. Zheludev, Supertoroidal light pulses as electromagnetic skyrmions propagating in free space, Nat. Commun. **12**, 5891 (2021).

[31] X. Lei, A. Yang, P. Shi, Z. Xie, L. Du, A. V. Zayats, and X. Yuan, Photonic spin lattices: Symmetry constraints for skyrmion and meron topologies, Phys. Rev. Lett. **127**, 237403 (2021).

[32] Z.-L. Deng, T. Shi, A. Krasnok, X. Li, and A. Alù, Observation of localized magnetic plasmon skyrmions, Nat. Commun. **13**, 8 (2022).

[33] H. Ge, X.-Y. Xu, L. Liu, R. Xu, Z.-K. Lin, S.-Y. Yu, M. Bao, J.-H. Jiang, M.-H. Lu, and Y.-F. Chen, Observation of acoustic skyrmions, Phys. Rev. Lett. **127**, 144502 (2021).

[34] R. D. Muelas-Hurtado, K. Volke-Sepúlveda, J. L. Ealo, F. Nori, M. A. Alonso, K. Y. Bliokh, and E. Brasselet, Observation of polarization singularities and topological textures in sound waves, Phys. Rev. Lett. **129**, 204301 (2022).

[35] L. Cao, S. Wan, Y. Zeng, Y. Zhu, and B. Assouar, Observation of phononic skyrmions based on hybrid spin of elastic waves, Sci. Adv. **9**, eadf3652 (2023).

[36] M. Yessenov, L. A. Hall, K. L. Schepler, and A. F. Abouraddy, Space-time wave packets, Adv. Opt. Photonics **14**, 455 (2022).

[37] Y. Shen *et al.*, Roadmap on spatiotemporal light fields, J. Opt. **25**, 093001 (2023).

[38] A. P. Sukhorukov and V. V. Yangirova, Spatio-temporal vortices: Properties, generation and recording, Proc. SPIE Int. Soc. Opt. Eng. **5949**, 594906 (2005).

[39] K. Y. Bliokh and F. Nori, Spatiotemporal vortex beams and angular momentum, Phys. Rev. A **86**, 033824 (2012).

[40] S. W. Hancock, S. Zahedpour, A. Goffin, and H. M. Milchberg, Free-space propagation of spatiotemporal optical vortices, Optica **6**, 1547 (2019).

[41] A. Chong, C. Wan, J. Chen, and Q. Zhan, Generation of spatiotemporal optical vortices with controllable transverse orbital angular momentum, Nat. Photonics **14**, 350 (2020).

[42] K. Y. Bliokh, Spatiotemporal vortex pulses: Angular momenta and spin-orbit interaction, Phys. Rev. Lett. **126**, 243601 (2021).

[43] X. Ding, P. Li, S.-C. S. Lin, Z. S. Stratton, N. Nama, F. Guo, D. Slotcavage, X. Mao, J. Shi, F. Costanzo, and T. J. Huang, Surface acoustic wave microfluidics, Lab Chip **13**, 3626 (2013).

[44] M. Wu, A. Ozcelik, J. Rufo, Z. Wang, R. Fang, and T. Jun Huang, Acoustofluidic separation of cells and particles, Microsyst. Nanoeng. **5**, 32 (2019).

[45] See Supplemental Material at http://link.aps.org/supplemental/10.1103/PhysRevLett.132.054003 for the derivation of Eqs. (1) and consideration of finite-depth effects as well as for the water-wave vortices and skyrmions formed by standing waves in closed reservoirs.

[46] M. F. Picardi, K. Y. Bliokh, F. J. Rodríguez-Fortuño, F. Alpeggiani, and F. Nori, Angular momenta, helicity, and other properties of dielectric-fiber and metallic-wire modes, Optica **5**, 1016 (2018).

[47] K. Y. Bliokh, Elastic spin and orbital angular momenta, Phys. Rev. Lett. **129**, 204303 (2022).

[48] S. J. van Enk and G. Nienhuis, Commutation rules and eigenvalues of spin and orbital angular momentum of radiation fields, J. Mod. Opt. **41**, 963 (1994).

[49] K. Y. Bliokh, M. A. Alonso, E. A. Ostrovskaya, and A. Aiello, Angular momenta and spin-orbit interaction of nonparaxial light in free space, Phys. Rev. A **82**, 063825 (2010).

[50] K. Y. Bliokh, M. R. Dennis, and F. Nori, Relativistic electron vortex beams: Angular momentum and spin-orbit interaction, Phys. Rev. Lett. **107**, 174802 (2011).

[51] K. Y. Bliokh and F. Nori, Spin and orbital angular momenta of acoustic beams, Phys. Rev. B **99**, 174310 (2019).

[52] W. L. Jones, Asymmetric wave-stress tensors and wave spin, J. Fluid Mech. **58**, 737 (1973).

[53] A. J. Vernon, M. R. Dennis, and F. J. Rodríguez-Fortuño, 3D Zeros in Electromagnetic Fields, arXiv:2301.03540.

[54] L. D. Landau and E. M. Lifshitz, *Fluid Mechanics* (Butterworth-Heinemann, Oxford, 1987).

[55] M. V. Berry and M. R. Dennis, Polarization singularities in isotropic random vector waves, Proc. R. Soc. A **457**, 141 (2001).

[56] K. Y. Bliokh, M. A. Alonso, and M. R. Dennis, Geometric phases in 2D and 3D polarized fields: Geometrical, dynamical, and topological aspects, Rep. Prog. Phys. **82**, 122401 (2019).

[57] J. F. Nye and J. V. Hajnal, The wave structure of monochromatic electromagnetic radiation, Proc. R. Soc. A **409**, 21 (1987).

[58] I. Freund, Optical Möbius strips in three-dimensional ellipse fields: I. Lines of circular polarization, Opt. Commun. **283**, 1 (2010).

[59] T. Bauer, P. Banzer, E. Karimi, S. Orlov, A. Rubano, L. Marrucci, E. Santamato, R. W. Boyd, and G. Leuchs, Observation of optical polarization Möbius strips, Science **347**, 964 (2015).

[60] T. S. van den Bremer and Ø. Breivik, Stokes drift, Phil. Trans. R. Soc. A **376**, 20170104 (2017).

[61] G. Falkovich, *Fluid Mechanics*, 2nd ed. (Cambridge University Press, Cambridge, England, 2018).

[62] M. E. McIntyre, On the 'wave momentum' myth, J. Fluid Mech. **106**, 331 (1981).

[63] R. Peierls, *Surprises in Theoretical Physics* (Princeton University Press, Princeton, NJ, 1979).

[64] R. Peierls, *More Surprises in Theoretical Physics* (Princeton University Press, Princeton, NJ, 1991).

[65] K. Y. Bliokh, Y. P. Bliokh, and F. Nori, Ponderomotive forces, Stokes drift, and momentum in acoustic and electromagnetic waves, Phys. Rev. A **106**, L021503 (2022).

[66] J. Masajada and B. Dubik, Optical vortex generation by three plane wave interference, Opt. Commun. **198**, 21 (2001).

[67] A. Ghosh, S. Yang, Y. Dai, Z. Zhou, T. Wang, C.-B. Huang, and H. Petek, A topological lattice of plasmonic merons, Appl. Phys. Rev. **8**, 041413 (2021).

[68] M. Król, H. Sigurdsson, K. Rechcińska, P. Oliwa, K. Tyszka, W. Bardyszewski, A. Opala, M. Matuszewski, P. Morawiak, R. Mazur, W. Piecek, P. Kula, P. G. Lagoudakis, B. Pietka, and J. Szczytko, Observation of second-order meron polarization textures in optical microcavities, Optica **8**, 255 (2021).

[69] A. Cazaubiel, F. Haudin, E. Falcon, and M. Berhanu, Forced three-wave interactions of capillary-gravity surface waves, Phys. Rev. Fluids **4**, 074803 (2019).

[70] S. Birkholz, C. Brée, I. Veselić, A. Demircan, and G. Steinmeyer, Ocean rogue waves and their phase space dynamics in the limit of a linear interference model, Sci. Rep. **6**, 35207 (2016).

[71] M. McAllister, S. Draycott, T. Davey, Y. Yang, T. Adcock, S. Liao, and T. Van den Bremer, Wave breaking and jet formation on axisymmetric surface gravity waves, J. Fluid Mech. **935**, A5 (2022).

[72] A. P. Abella and M. N. Soriano, Measurement of Eulerian vorticity beneath rotating surface waves, Phys. Scr. **95**, 085007 (2020).

[73] A. P. Abella and M. N. Soriano, Spatio-temporal analysis of surface waves generating octupole vortices in a square domain, J. Exp. Theor. Phys. **130**, 452 (2020).

[74] A. P. Abella, Vorticity of wave-based octupole metamaterials, Mater. Lett. **283**, 128720 (2021).